INTERNATIONAL JOURNAL OF CLIMATOLOGY
Int. J. Climatol. (2014)
Published online in Wiley Online Library
(wileyonlinelibrary.com) DOI: 10.1002/joc.3943

RMetS
Royal Meteorological Society

Surface air temperature patterns on a decadal scale in China using self-organizing map and their relationship to Indo-Pacific warm pool

Haixia Shan,[a,b] Yuping Guan[b]* and Jianping Huang[a]

[a] *Key Laboratory for Semi-Arid Climate Change of the Ministry of Education, College of Atmospheric Science, Lanzhou University, 730000, China*

[b] *State Key Laboratory of Tropical Oceanography, South China Sea Institute of Oceanology, Chinese Academy of Sciences, Guangzhou, 510301, China*

ABSTRACT: In this study, nine decadal-scale surface air temperature (SAT) patterns in China during 1902–2007 were obtained from Climatic Research Unit data using the self-organizing map based on the ensemble empirical mode decomposition. To further investigate the relationship between decadal SAT patterns in China and the Indo-Pacific warm pool (IPWP), we aggregated the selected nine neurons into three significant types based on the similarities of the reference vectors using a hierarchical agglomerative clustering approach. Among the three patterns, Pattern 1 is a cold pattern and Pattern 3 is a warm pattern. Pattern 2 is a medium mode, in which the west of China is cold, but eastern China is warm. The relationship between the IPWP and SAT in China at the decadal scale can be summarized as follows. When the IPWP is warmer, easterly wind anomalies are stronger over the equatorial Pacific Ocean, the IPWP shrinks westwards predominantly and the heat centre is to the west. Furthermore, easterly wind anomalies strengthen the trade winds, so that poleward energy transport by the ocean increases, while poleward energy transport by the atmosphere decreases in the tropics. Meanwhile, the Aleutian Low and East Asian trough strengthen, and the meridional circulation is dominated, which is of benefit to cold air from the high latitude that move to the southeast, making the temperature in China colder. In contrast, the warm pool is colder, and the westerly wind anomalies are prevailing, making the IPWP extending eastward. Zonal circulation is dominant in the mid-latitudes, which weakens the cold airflow into China and leads to warmer temperatures there.

KEY WORDS surface air temperature; Indo-Pacific warm pool; self-organizing map; ensemble empirical mode decomposition

Received 8 July 2013; Revised 4 January 2014; Accepted 7 January 2014

1. Introduction

Temperature is an important meteorological variable, and is related to solar radiation and both evaporation and transpiration, which constitute important elements of the hydrological cycle. Decadal variability forms the background to interannual climate changes, and is important for interannual climate prediction and long-term national economic development planning. Interdecadal climate variation has attracted significant attention from both domestic and international climate and ocean scientists, and has become a hot topic in climate research. Using a singular spectrum analysis on global surface temperature records, Schlesinger and Ramankutty (1994) identified a temperature oscillation with a period of 65–70 years and suggested that it arises from internal ocean–atmosphere variability. Jiang *et al.* (2001) used multitaper spectral analysis to identify significant multidecadal variations with periods of about 40–70 years, which are superimposed on a linear warming trend for the Northern Hemisphere mean temperature. Tang *et al.* (2010) aggregated 10 regional surface air temperature (SAT) series in China (Wang *et al.*, 1998, 2004) from 1880 to 2002, and found three significant decade-long warming intervals (1920s, 1940s, and 1990s), as well as an extended phase of relative cooling between the 1950s and early 1980s. The 1920s and 1940s warming is most likely naturally induced (e.g. Wood and Overland, 2010). By contrast, the rapid warming since the mid-1980s (Wang and Gong, 2000) has raised the possibility of early detection of the imprints of anthropogenic CO_2.

Climate variability or changes are often considered from the standpoint of the climate anomaly; i.e. the deviation from the annual cycle. The above-mentioned research was all based on this traditional approach; however, climate change is not only reflected in the change in the annual mean of a climate variable, but also in the long-term change in the amplitude and phase of its annual cycle (e.g. Thomson, 1995; Stine *et al.*, 2009; Qian *et al.*, 2011a, 2011b). Wu *et al.* (2008) proposed

* Correspondence to: Y. Guan, South China Sea Institute of Oceanology, Chinese Academy of Sciences, Guangzhou 510301, China. E-mail: guan@scsio.ac.cn

an alternative reference frame for climate anomalies: the modulated annual cycle (MAC), which uses the empirical mode decomposition (EMD) and ensemble empirical mode decomposition (EEMD) methods that allow the annual cycle to change from year to year. The effectiveness of the EMD–EEMD method has recently been shown in many geophysical applications (e.g. Huang and Wu, 2008; Wu *et al.*, 2008; Qian *et al.*, 2009, 2010, 2011a, 2011b, 2011c; Ruzmaikin and Feynman, 2009; Wu and Huang, 2009; Franzke, 2010; Breaker and Ruzmaikin, 2011; Franzke and Woolings, 2011). Qian *et al.* (2010) raised the even more fundamental issue of the need for a proper reference frame, arguing for the use of MAC as opposed to the traditional focus on anomalous changes in the mean climatology over time. This provides for a more physics-based study of the multi-timescale variability of SAT in China.

There are many meteorological and climatic processes that can influence the temperature in China, such as the El Niño/Southern Oscillation (ENSO) (e.g. Wu *et al.*, 2010), North Atlantic Oscillation (e.g. Sun *et al.*, 2008), Arctic Oscillation (e.g. Huang *et al.*, 2007), Pacific decadal oscillation (e.g. Zhu and Yang, 2003), sea surface temperature (SST) in the Indian Ocean (e.g. Xie *et al.*, 2009), the stratosphere–troposphere exchange (e.g., Yu *et al.*, 2004), the Siberian High (Gong and Ho, 2002b), and surface solar radiation (Qian *et al.*, 2011a). The Indo-Pacific warm pool (IPWP) is the major region of atmospheric convection, and the major source of heat driving global atmospheric circulation (Gadgil *et al.*, 1984). Changes of the warm pool can alter atmospheric divergent flow locally, and affect the Walker and Hadley circulations, causing a global climate response (Sardeshmukh and Hoskins, 1988; Neale and Slingo, 2003). Furthermore, many previous studies focussed on the general features of the climate in China as a whole, rather than spatial distribution patterns. Decadal-scale SAT patterns over the entire 20th century in China have received little attention. Here, we focus mainly on the relationship between the IPWP and the decadal patterns of SAT in China obtained from the self-organizing map (SOM) technique (Kohonen, 1982, 2001). To investigate the influence of IPWP, we also defined four specific properties of the warm pool: the volume of the warm pool, together with the longitudinal, latitudinal, and vertical locations of its heat centre (HC). Firstly, we used the EMD–EEMD method to extract the decadal component of SAT and the four indices. The decadal component of each SAT grid in China was then categorized into the most common patterns of variability using the SOM clustering technique. To further investigate the relationship between decadal SAT patterns in China and the IPWP, we aggregated the selected nine neurons into three significant types. The detailed patterns of SAT and the state of the

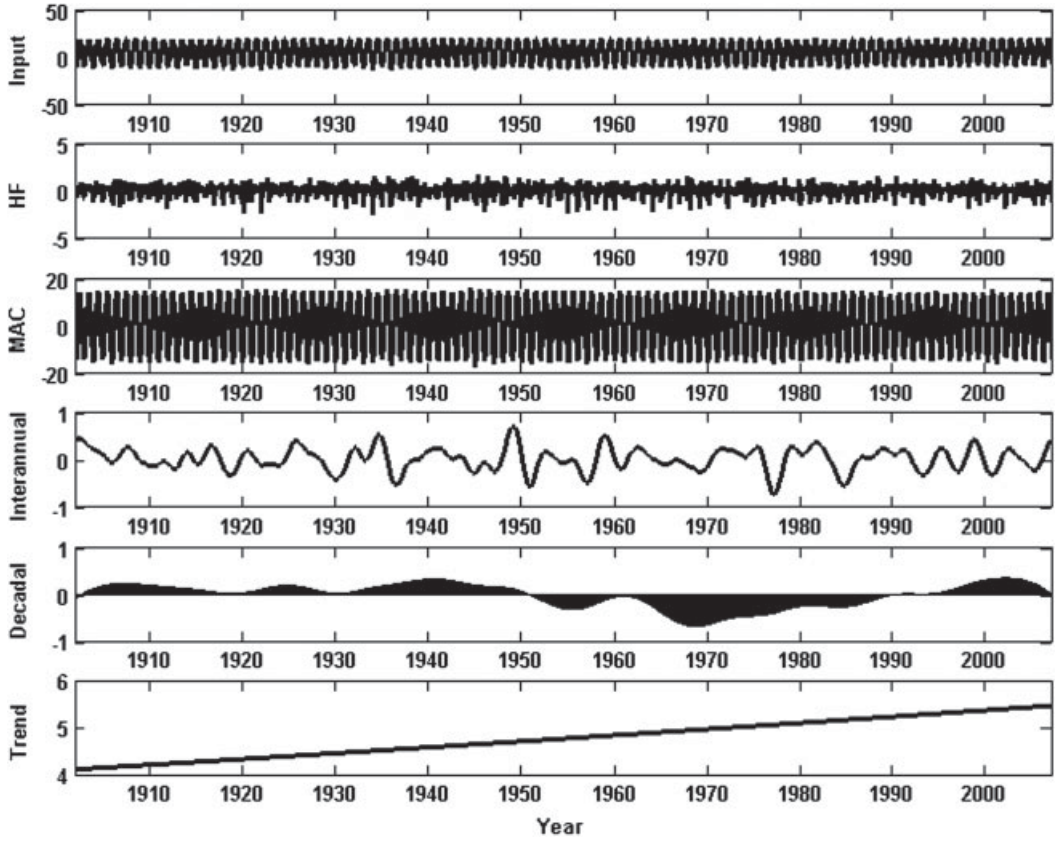

Figure 1. Decomposition and reconstruction of the mean surface air temperature in China from January 1902 to December 2007. 'Input' stands for the raw monthly series.

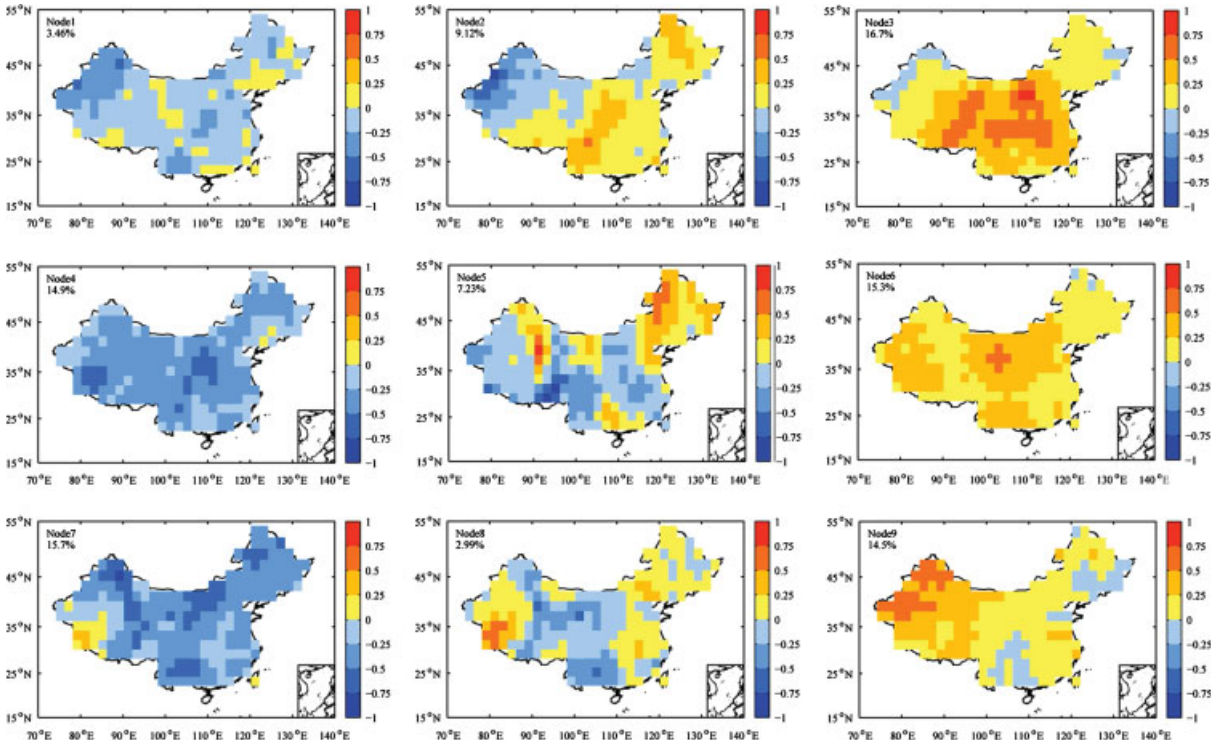

Figure 2. Decadal SAT patterns and their occurrence frequency in China using self-organizing maps (SOM).

IPWP from the four indexes in every mode are displayed. The vertical structure of the ocean and atmospheric circulation in the three patterns are also shown.

2. Data and methods

2.1. Data

The Climatic Research Unit (CRU; University of East Anglia, UK) land-SAT time series (CRU TS 3.10) used in this study is the new version of the dataset developed by the CRU. It contains monthly grids of observed climate data for the period 1901.1–2009.12, and covers the global land surface on a $0.5^\circ \times 0.5^\circ$ grid, including oceanic islands, but excluding Antarctica. More detailed descriptions of the datasets are given in Mitchell and Jones (2005) and Harris *et al.* (2013). Wen *et al.* (2006) compared the CRU data with domestic observations in the 10 regions of China defined by Wang *et al.* (1998, 2004), and found good agreement, apart from that in the Tibet and Xinjiang areas. This suggests that the CRU high-resolution grid data can provide a reasonably complete picture of climate change in China during the 20th century.

The data used to compute the size and HC of IPWP were obtained from the Simple Ocean Data Assimilation (SODA) 2.2.4, which is available from 1871 to 2008 (Giese and Ray, 2011). The ocean model was based on Parallel Ocean Program, with an average resolution of $0.25^\circ \times 0.4^\circ \times 40$ levels. The ocean model surface boundary conditions were provided by a new atmospheric dataset (Compo *et al.*, 2011) designated as Twentieth Century Reanalysis version 2 (20CRv2). The surface wind stress from 20CRv2 was used in the ocean model for the surface momentum fluxes, and solar radiation, specific humidity, cloud cover, 2-m air temperature, precipitation, and 10-m wind speed were used to determine the heat and fresh water fluxes. Observations include virtually all available hydrographic profile data, as well as ocean station data, moored temperature and salinity time series, surface temperature and salinity observations of various types, and nighttime infrared satellite SST data. The output is in monthly-averaged form, mapped onto a uniform $0.5^\circ \times 0.5^\circ \times 40$-level grid. To facilitate comparison between the SAT and IPWP, we used the two datasets from the period 1901.1–2008.12.

2.2. Methods

Following the main procedures in Wu *et al.* (2008), we use an adaptive and temporally local data analysis tool – the EEMD (Wu and Huang, 2009) method to extract the decadal component of SAT. We reconfigured the mean SAT in China into five major timescale components (Figure 1): the high-frequency component (HF in Figure 1, representing intra-annual variability); the MAC component (MAC in Figure 1); the interannual timescale component (interannual in Figure 1); the decadal component (decadal in Figure 1); and the trend component (trend in Figure 1). Similarly, we reconfigured the SAT in every grid in China as above. To eliminate the minor influence of end effects on the results, the first and last

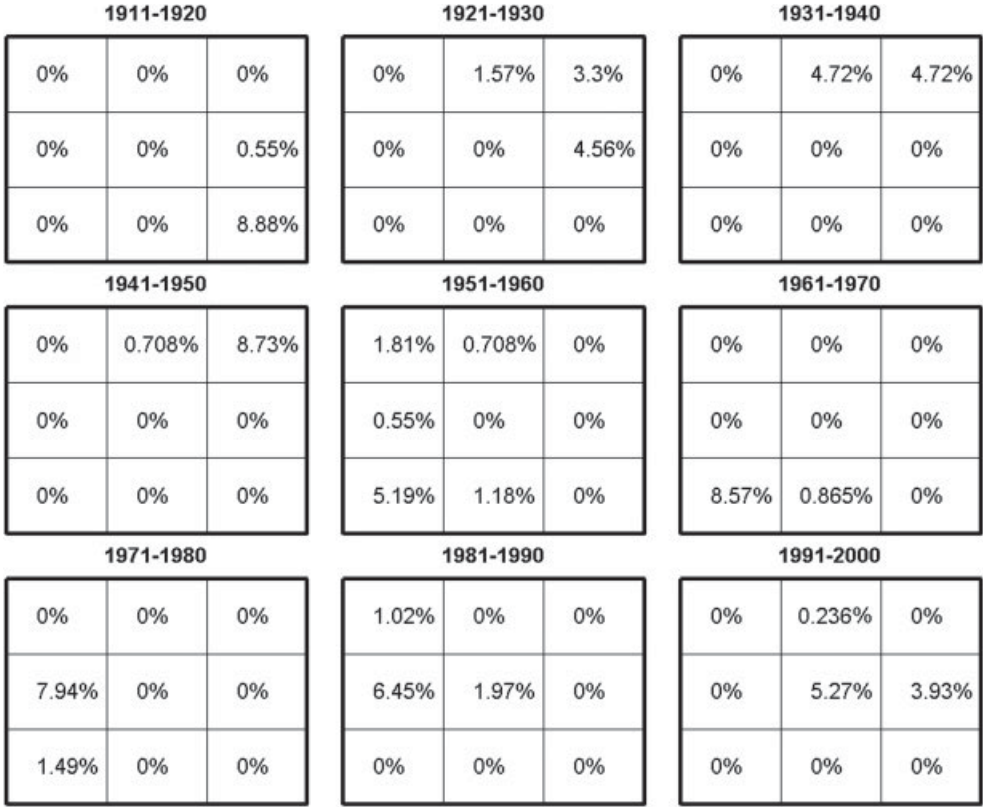

Figure 3. Decadal frequency maps of the 3*3 SOM array. They show the occurrence frequency (in %) of each SAT patterns shown in Figure 2 for each decade.

years of all of the decomposed results were excluded, leaving the period 1902–2007 to be analysed.

The IPWP volume, and the longitudinal, latitudinal, and vertical locations of the HC of the warm pool were calculated in the region enclosed by the 28 °C isotherm within the region between 30°S–30°N and 30°E–120°W. An HC X_i ($i = 1, 2, 3$) was defined following the method of Chen and Fang (2005):

$$X_{\mathrm{i}} = \frac{\sum_{\mathrm{j}=1}^{n} w_j X_{ij}}{\sum_{j=1}^{n} w_j}, i = 1, 2, 3, \quad (1)$$

$$w_j = \frac{T_j\text{-}T_{\min}}{T_{\max}\text{-}T_{\min}}. \quad (2)$$

Here, the factor i denotes the zonal ($i = 1$), meridional ($i = 2$), and vertical ($i = 3$) directions, n is the number of grid points in the warm pool, and T_j is the temperature of seawater at point j. X_{ij} is X_i of the sea water at point j, and w_j is a normalized weighting function. Consequently, X_i ($i = 1, 2, 3$) indicates the longitude, latitude, and depth of the HC of the warm pool, respectively.

The SOM algorithm was first described by Kohonen (1982) for reducing the dimensions of large datasets to enable the visualization and interpretation of the data characteristics. Details of the approach, which is closely followed here, are given by Cassano *et al.* (2006). The SOM has been shown to be more powerful than conventional methods (e.g. the empirical orthogonal functions) for feature extraction purposes (e.g. Reusch *et al.*, 2005; Liu *et al.*, 2006). It has been increasingly applied to meteorology, oceanography, and climate

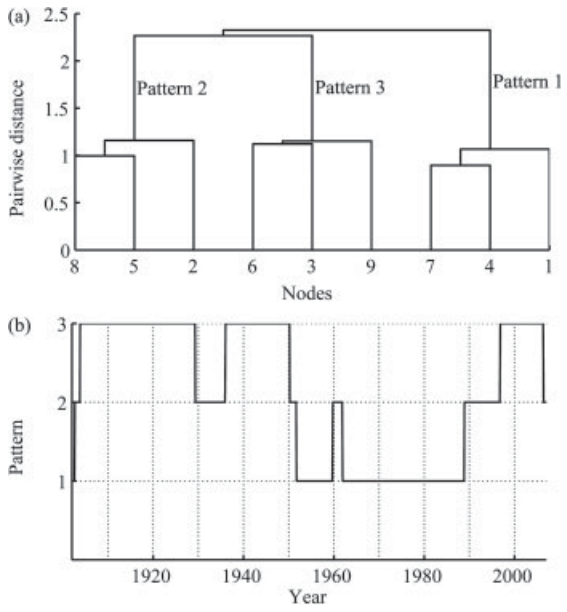

Figure 4. Dendrogram (a) of the decadal patterns of SAT in China using HAC and the clusters time series (b).

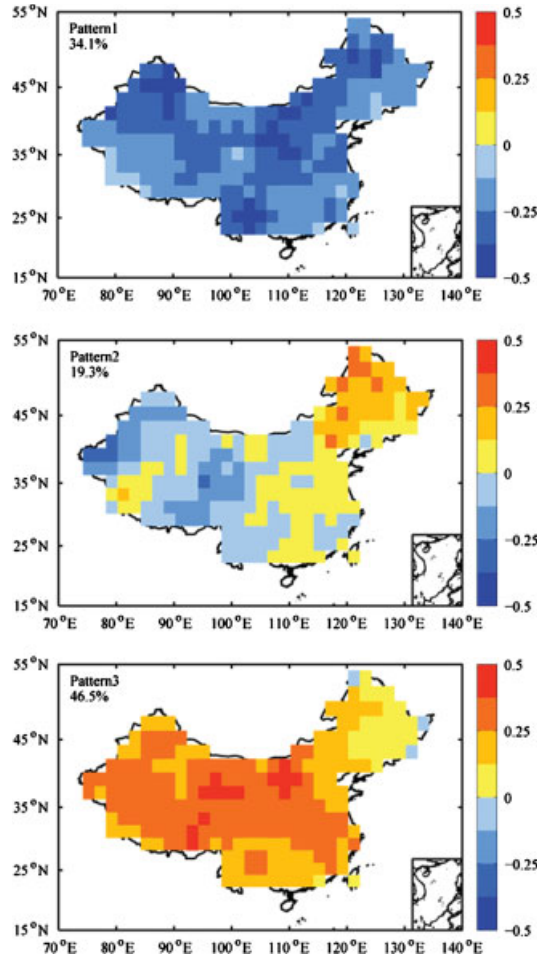

Figure 5. Three aggregated decadal SAT patterns and their occurrence frequency in China.

sciences (Liu and Weisberg, 2011). The output of the algorithm is a map of neurons that are associated with the input data via weights vectors, called prototype or reference vectors. These prototype vectors are a summary of

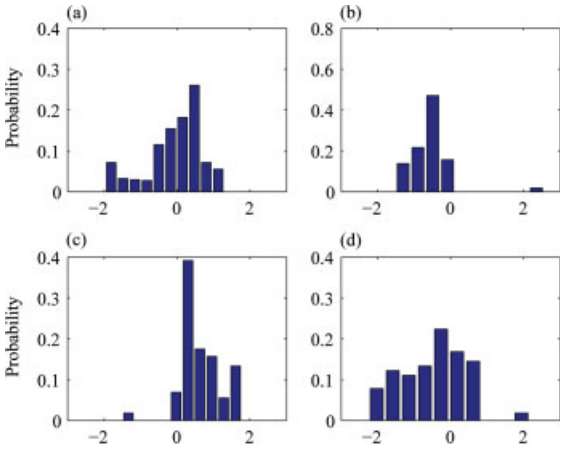

Figure 6. Probability distribution function of the decadal IPWP volume index (a), zonal HC index (b), meridional HC index (c), and vertical HC index (d) when Pattern 1 occurs.

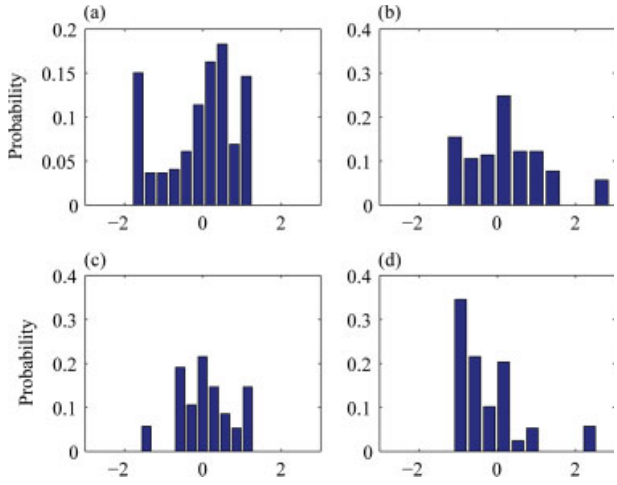

Figure 7. Probability distribution function of the decadal IPWP volume index (a), zonal HC index (b), meridional HC index (c), and vertical HC index (d) when Pattern 2 occurs.

situations. SOM algorithm produced a one-dimensional set of patterns or 'nodes' of SAT. Recently, a more user-friendly implementation of the SOM as a MATLAB Toolbox provided by Vesanto *et al.* (2000) facilitates our study. The SOM toolbox version 2.0 can be downloaded from the Helsinki University of Technology, Finland: http://www.cis.hut.fi/projects/somtoolbox. We use the batch training algorithm, because it is computationally more efficient than the sequential algorithm (Vesanto *et al.*, 1999, 2000). The neighbourhood function adopted is 'ep' which gives the most accurate patterns (Liu *et al*., 2006) is used, and all the other parameters used are the default ones in the SOM Toolbox. After testing several different numbers of nodes, it was found that nine nodes provided sufficient patterns to cover most aspects

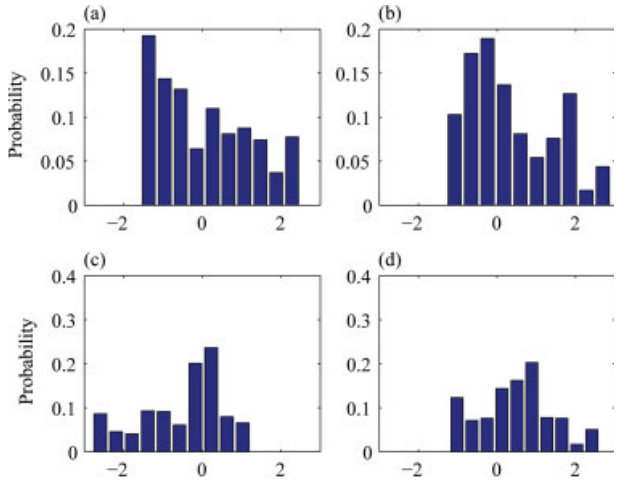

Figure 8. Probability distribution function of the decadal IPWP volume index (a), zonal HC index (b), meridional HC index (c), and vertical HC index (d) when Pattern 3 occurs.

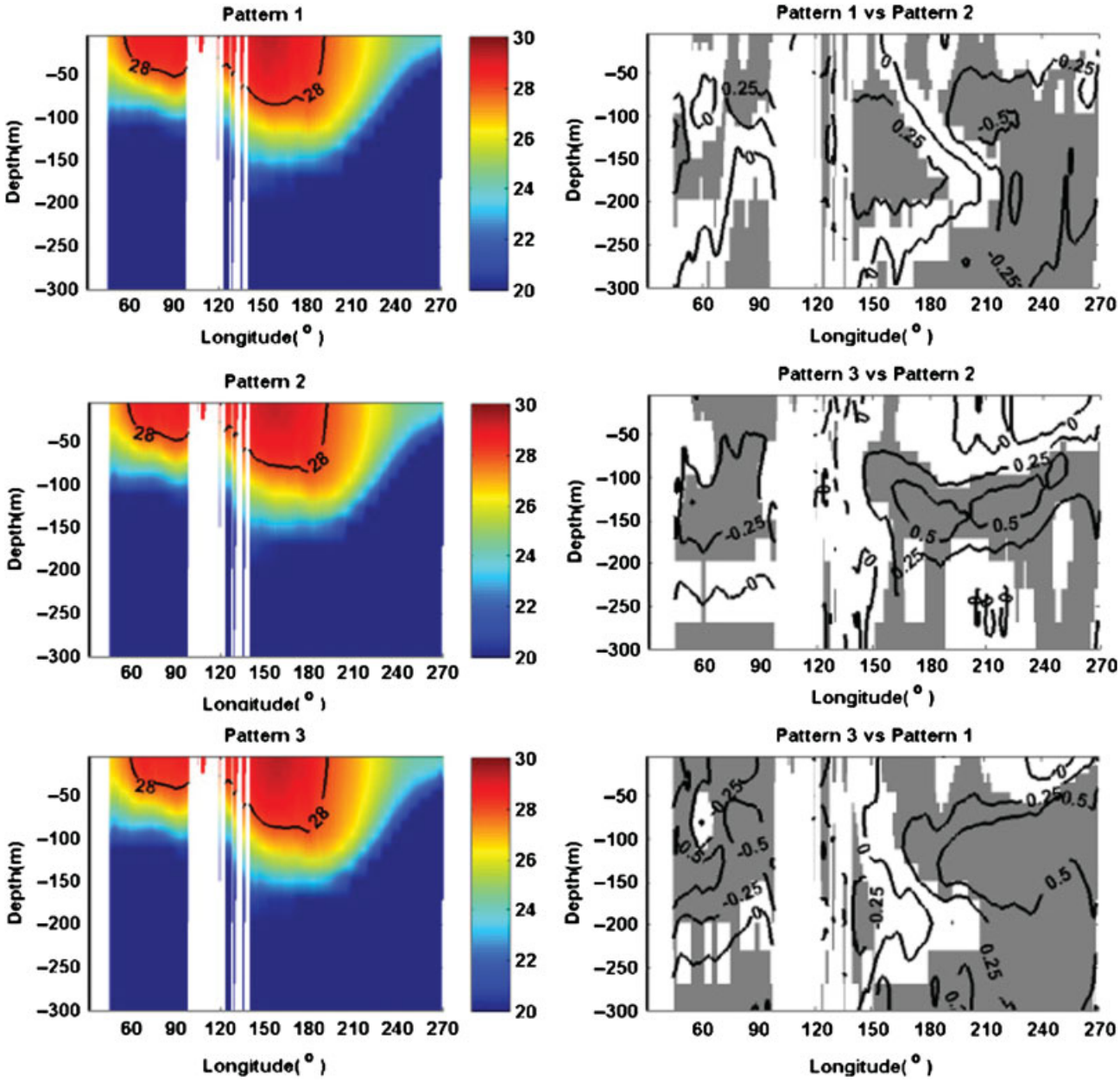

Figure 9. The mean ocean temperature over 2.5°S–2.5°N in three patterns (left panel) and the differences among the three patterns (right panel). Thick black and pink lines are 28 °C isothermal in each pattern. Dark shadings indicate temperature differences at the 5% significance level.

of decadal SAT variability, while also ensuring that each node was able to provide robust statistics for the properties of SAT.

3. Results

3.1. Decadal-scale SAT patterns in China

The decadal-scale patterns of SAT in China produced by the SOM algorithm and their occurrence frequencies are shown in Figure 2. The third node appears most frequently (16.75%), although all nodes are approximately equally distributed (except node 1 and node 8). It is cold in most parts of China in node 1, especially in Xing Jiang and most of Yunnan province. Node 2 shows that it is cold in northwest China, but it is warm in the east of China, and especially in southwest and northeast China. The third node shows that it is warm in most parts of China, except the northeast and northwest. In node 4, it is cold in most parts of China, especially in northern China and Tibet. Node 5 shows that it is cold in most parts of China, except in the northwest and northeast. Node 6 is also a warm pattern, and it is much warmer in parts of northwest and central China. It is cold in most parts of China, except south of Tibet, in node 7. Node 8 occurs least frequently (2.99%), but the warmer regions expand compared with pattern 7, and it is warm in the Yangtze River valley and most of northeast China.

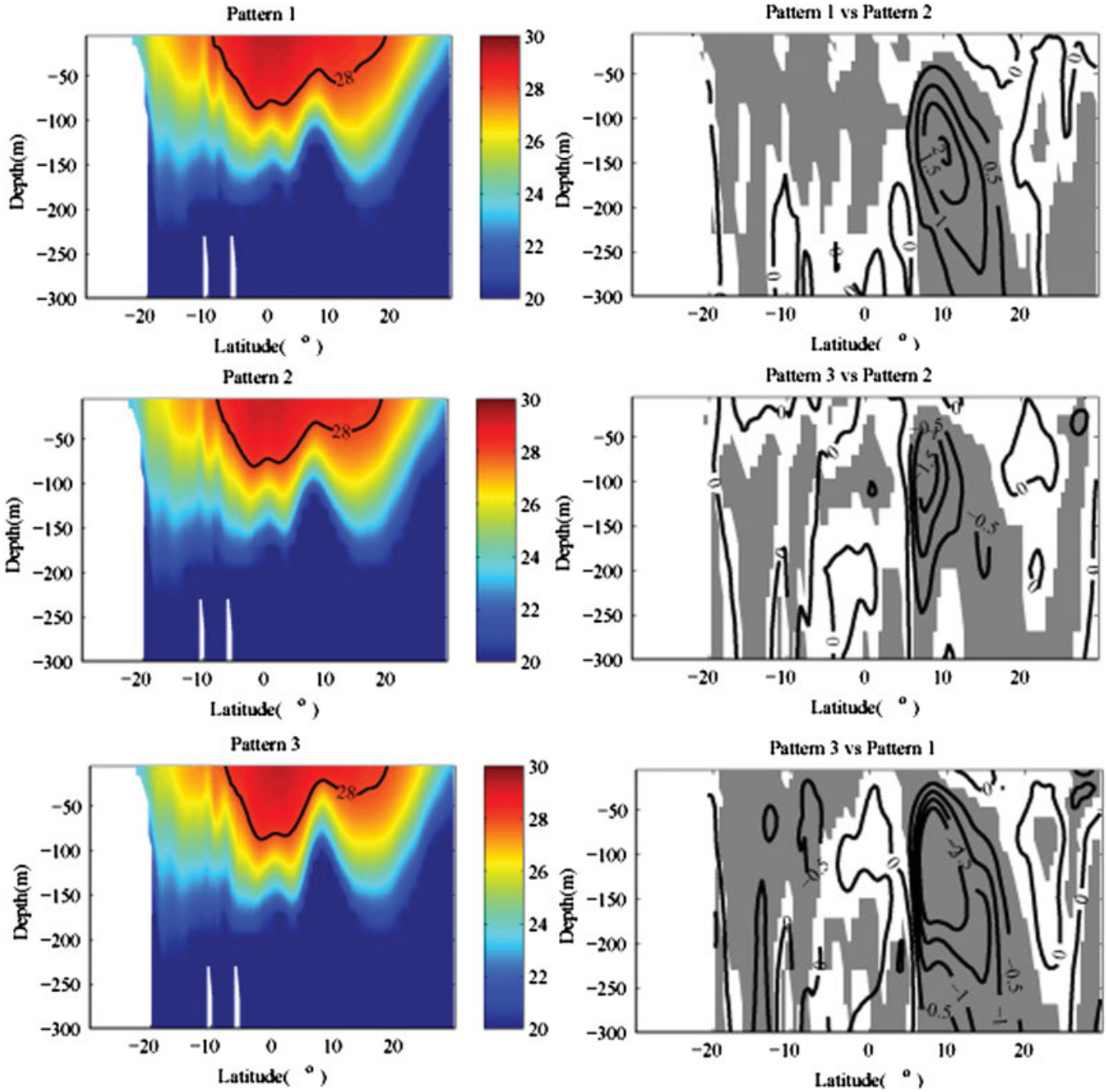

Figure 10. The latitude–depth cross section at 150°E in three patterns (left panel) and the differences among the three patterns (right panel). Thick black and pink lines are 28 °C isothermal in each pattern. Dark shadings indicate temperature differences at the 5% significance level.

Node 9 shows a warm pattern, especially in northwest China.

The SOM also successfully captured the remarkable decadal variation as shown in Figure 3. During the 1910s, China was mainly covered by node 9, in which the warm state of northwest China is evident. In addition, there were still some periods in which node 6 developed, which is also a warm pattern, with its warmest regions located mainly in north China, southwest China, and parts of Xinjiang and Tibet. Wen *et al.* (2006) described SAT changes based on the temperature anomaly every 10 years before the 1950s. In the 1910s, the SAT began to rise, but it was still cold in eastern China, and this differs from our results. During the 1920s, the occurrence frequency of node 6 begins to increase, rising from 0.55% to 4.56%. The occurrence frequency of node 3 also increases to 3.3%, which is also a warm pattern, except for northeast and northwest China. This is similar to the results of Wen *et al.* (2006). During the 1930s, the occurrence frequency of nodes 2 and 3 were the same, but Wen *et al.* (2006) found node 2 to be much more prominent. However, in the 1940s the occurrence frequency of node 2 decreased to about 0.7%, and node 3 dominated, which means that it was much warmer during this decade, and it was, in fact, the warmest decade of the first half of the 20th century. During the 1950s and 1960s, node 7 was the most common, and this is a cold pattern, while in the 1970s and 1980s node 4 dominated, and in the 1990s

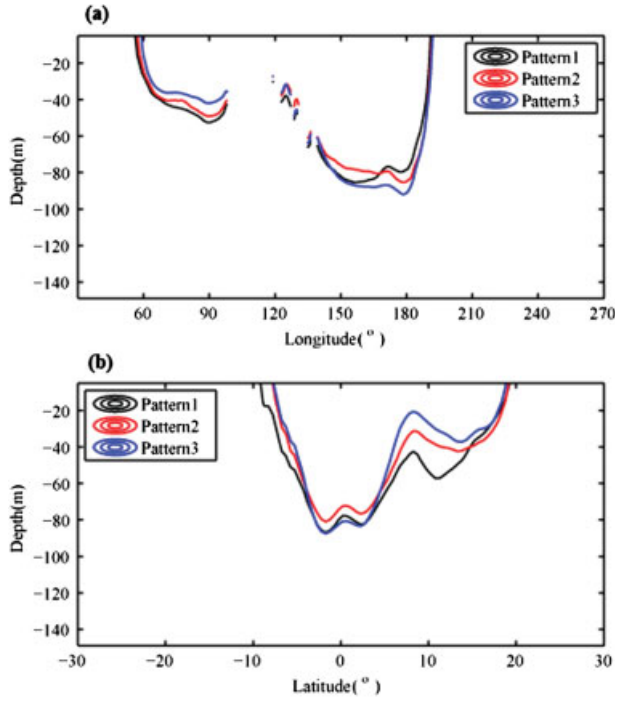

Figure 11. The comparison of the shape of IPWP in the three patterns. (a) Over 2.5°S–2.5°N, (b) a latitude–depth cross section at 150°E.

node 5 was the major pattern. Therefore, in the 1970s to 1980s it was cold, but there was a shift to a warm phase in the 1990s. However, during the 1940s the warm centre was in the central region of China, but it was in the northeast, Inner Mongolia, and the Xinjiang area in the 1990s. China experienced two warm periods in the 1940s and 1990s in the 20th century, but which of the two was the warmer remains controversial. Some researchers believe that it was warmer in the 1990s (Chen *et al.*, 2004), while others think the opposite (Ding and Dai, 1994). During the 1990s, node 5 dominated (5.27%), so that the warm phase mainly occurred in northeast China, and most of the rest of China was cold. In the second major pattern (node 6), the amplitude of the warming is much smaller than that in node 3. However, in 1940s there are 2 nodes (node2, node 3) happening, and node 3 dominated (92.5%).Therefore, the magnitude of the warming in the 1940s was much more distinct at the decadal scale.

To investigate the decadal SAT pattern further, we aggregated the nine nodes into three significant types based on the similarities of the reference vectors using a hierarchical agglomerative clustering (HAC; Jain and Dubes, 1988) algorithm. The HAC approach is used to obtain a classification such that each reference vector belonging to a cluster is as close as possible to the other reference vectors of this cluster, and as far as possible from the reference vectors belonging to any other cluster. In the dendrogram shown in Figure 4(a), each leaf of the tree is a subset of neurons, and each node of the tree represents the conjunction of two clusters, with the size of its branches being representative of the distance between two clusters. In Figure 2, nodes 1, 4, and 7 are under a cold condition, and we aggregated them as Pattern 1. In nodes 2, 5, and 8, it is warm in eastern China but cold in western China, based on the aggregated decadal SAT pattern (Figure 5), and we refer to this scenario as Pattern 2. Pattern 3 is the aggregate of nodes 3, 6, and 9, and this pattern is a warm pattern in which the western part of China is much warmer. From the cluster time series (Figure 4(b)) we see that before 1950, China is warm on a decadal scale, but that it changes to a cold mode from then on, until shifting back to a warm pattern after the 1990s. This sequence differs from the results of previous studies (e.g. Graham, 1994; Hu, 1997; Gong and Ho, 2002a) based on the anomaly series, which all found an abrupt change in rainfall and temperature variations around the late 1970s. However, it is similar with the result of surface temperature in North China (Qian and Zhou, 2013).

3.2. Status of the IPWP during different SAT patterns in China

To investigate the relationship of the status of the IPWP with the SAT pattern in China, we normalized the four IPWP indices defined in Section 2 and then calculated the probability distribution when the three patterns occur. Figures 6–8 show the decadal component of the four indexes in the three patterns. Under Pattern 1, the IPWP tends to have a larger volume, and its HC is to the northwest and is shallower. In addition, the probability that the zonal and meridional location of the HC is to the northwest is greater than 0.9. In the medium pattern (Pattern 2), the IPWP has a larger volume, and the HC is to the southeast and is shallower. The difference between the cold pattern and medium pattern is that the zonal and meridional locations of the HC are reversed. In the warm pattern (Pattern 3), the IPWP has a smaller volume, with its HC located to the southeast and deeper. The difference between the warm pattern and medium pattern is that the volume and vertical location of the HC are reversed.

The above probability distribution of the four indexes in each pattern gives the general characteristics of the IPWP in the three patterns. To further investigate corresponding changes in oceanic circulations associated with each pattern, Figure 9 shows the vertical structure of the ocean temperature averaged between 2.5°S and 2.5°N for the three patterns, as well as the mutual differences among the three patterns. The distance between two intersections of the 28°C isotherm with the ocean surface can be taken as an approximate zonal dimension of the IPWP near the equator (Wang and Metha, 2008). The difference between Patterns 1 and 2 is that the equatorial western Pacific is much warmer, especially between 100 and 200 m, and it is much colder in the eastern Pacific. In the Indian Ocean the upper level is warmer, and it is colder below 150 m. Considering the difference between Patterns 3 and 2, the temperature between 100 and 200 m in the eastern and middle Pacific is much warmer, but it is much colder at the same depth in the Indian Ocean. In Pattern 3, it is colder in the Indian

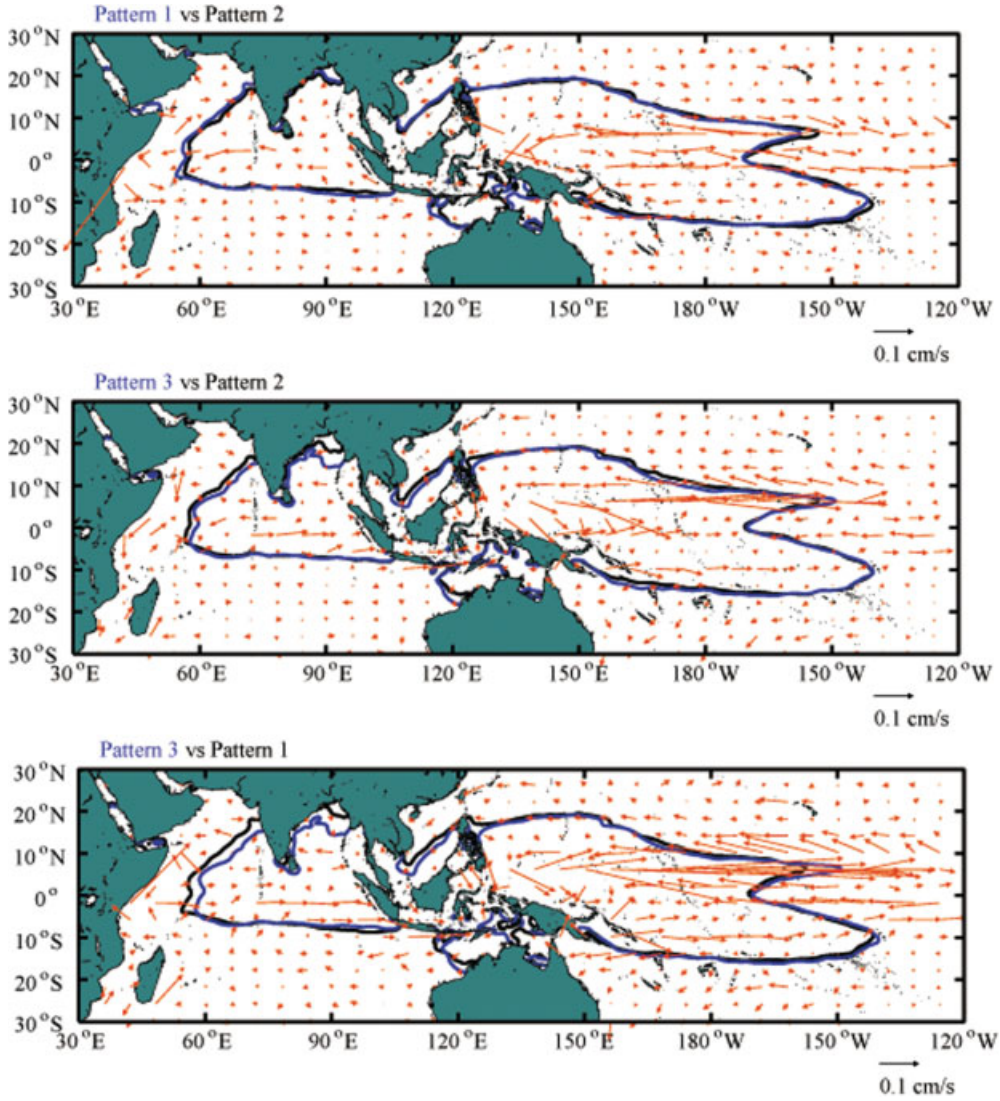

Figure 12. The ocean current at 5-m depth differences among the three patterns. Black and blue lines indicate temperature greater than 28°C.

Ocean above 200 m, and the warming in the eastern and middle Pacific is much stronger, but it is colder in the western Pacific than in Pattern 1.

A similar vertical-meridional cross-section for ocean temperature along 150°E longitude is shown in Figure 10, where the IPWP has the maximum meridional extension. The main difference between Pattern 1 and Pattern 2 is that it is much warmer in the region 10°–20°N in Pattern 1. Regarding the difference between Patterns 3 and 2, it is much colder in the region 10°–20°N in Pattern 3. The main difference between Pattern 3 and Pattern 1 is the same as that between Patterns 3 and 2, only the difference is much more pronounced. The temperature change in the region 10°–20°N has a significant influence on the shape of the north branch of the IPWP.

A detailed comparison of the shape of the IPWP in the three patterns is shown in Figure 11. The eastward extension of the IPWP shows little difference in the three patterns. In Pattern 1, the westward extension of IPWP and the vertical expanding in the Indian Ocean are largest of all the three patterns. In addition, the north branch is deepest and the southward extension of the south branch of the IPWP is also the largest. In Pattern 2, the south branch of the IPWP is shallowest and the northward extension of the north branch is strongest. In Pattern 3, the vertical extension in the Indian Ocean is shallowest, but it is deepest in the western Pacific. Furthermore, the vertical extension of the northern branch is shallowest, and the southern branch is deepest and farthest north.

To explore the dynamical processes responsible for the IPWP decadal variability, Figure 12 shows the mutual differences of ocean current at a depth of 5 m among the three patterns. Strong anomalous surface currents are found in the equatorial Pacific and Indian Ocean, and weak anomalous currents are found in the subtropics. Strong westerly flows in Pattern 1 relative to Pattern 2 in the central Pacific and the Indian Ocean increase the zonal expansion of the Indian Ocean warm pool (IOWP) and cause the western Pacific warm pool (WPWP) to shrink. Therefore, the HC of the IPWP is to the west. In Pattern 3, the anomalous easterly flows (compared with Pattern

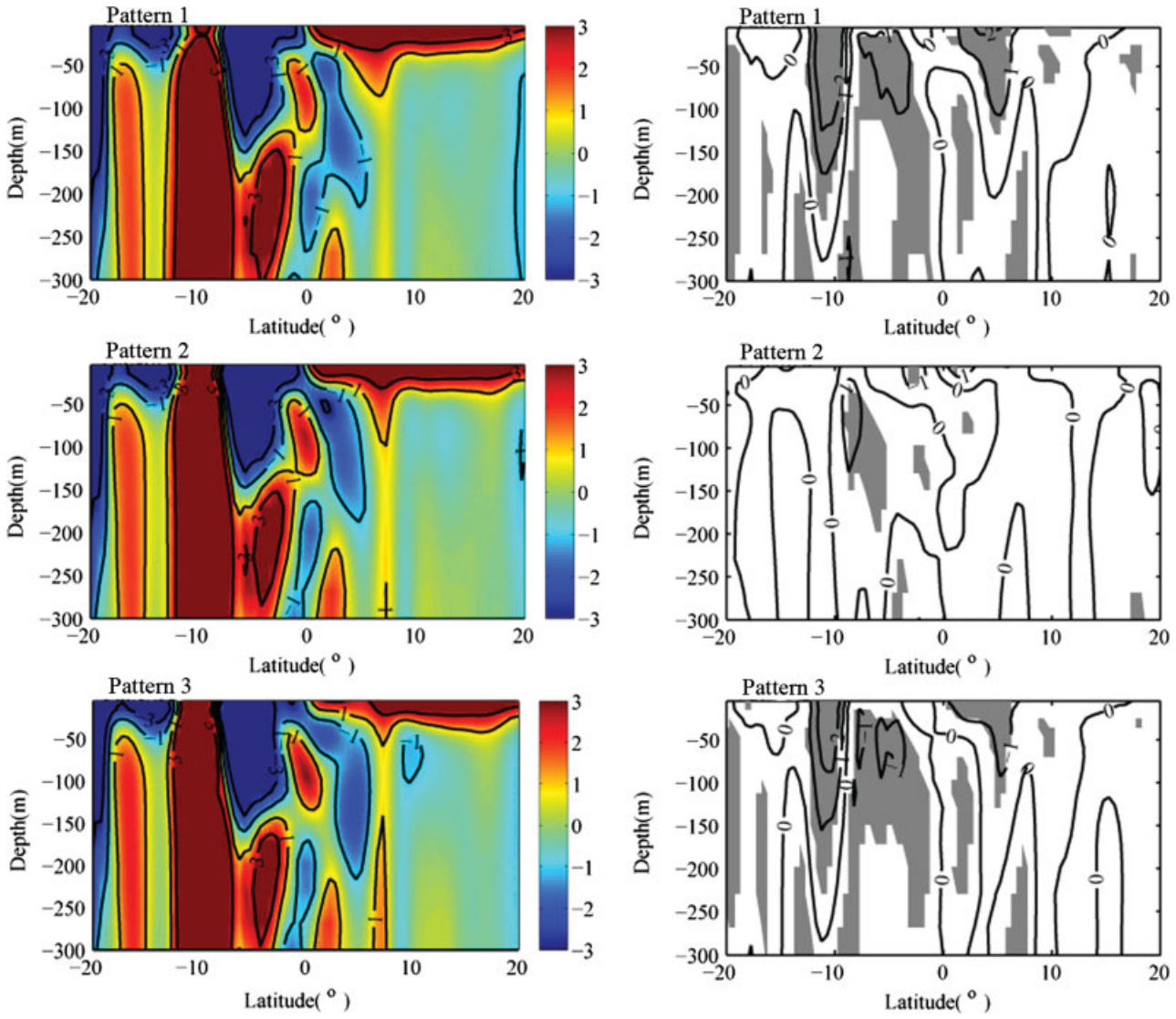

Figure 13. Anomalous meridional velocity at 150 °E–155°E and the differences compared with the mean value (1902–2007). Dark shadings indicate velocity differences at the 5% significance level.

2) cause the IOWP to shrink and the WPWP to expand to the east, causing the HC of the IPWP to move to the east. In addition, the southern extension of the northern boundary is evident. The anomalous distribution between Patterns 3 and 1 is similar to that between Patterns 3 and 2, only the amplitude is much greater.

The upper-ocean circulation in the tropical Pacific can be described in terms of shallow subtropical–tropical overturning cells (STCs; Liu, 1994; McCreary and Lu, 1994). The mainly wind-driven cells appear in the zonal integral as closed cells with an upwelling at the equator, a poleward Ekman transport at the surface, subduction in the subtropics, and an equatorward flow within the thermocline. Figure 13 shows a vertical cross-section of mean meridional velocity at 150°–155°E associated with the three patterns, and their differences relative to the mean condition (1902–2007). The Southern Hemisphere STC is weaker and the Northern Hemisphere STC strengthens in Patterns 1 and 2. In Pattern 3, the Southern Hemisphere STC strengthens and the Northern Hemisphere STC weakens. Stronger STCs may lead to a stronger subduction and warming of the ocean temperature under the surface. In Patterns 1 and 2, for example, a weaker Southern Hemisphere STC can cool the warm pool in the Southern Hemisphere while a stronger Northern Hemisphere STC warms the warm pool in the Northern Hemisphere, causing the HC to move to the north. The changes in Pattern 3 are the opposite of this situation. In addition, the Southern Hemisphere STC is stronger than the Northern Hemisphere STC, the vertical HC of the IPWP is mainly determined by the Southern Hemisphere STC in Patterns 1 and 2, and the Southern Hemisphere STC is weaker, so the HC tends to be shallower. The corresponding condition in Pattern 3 is the opposite of this scenario.

The corresponding geopotential height difference at 500 hPa, compared with the average (1902–2007) for the three patterns, is shown in Figure 14. In Pattern

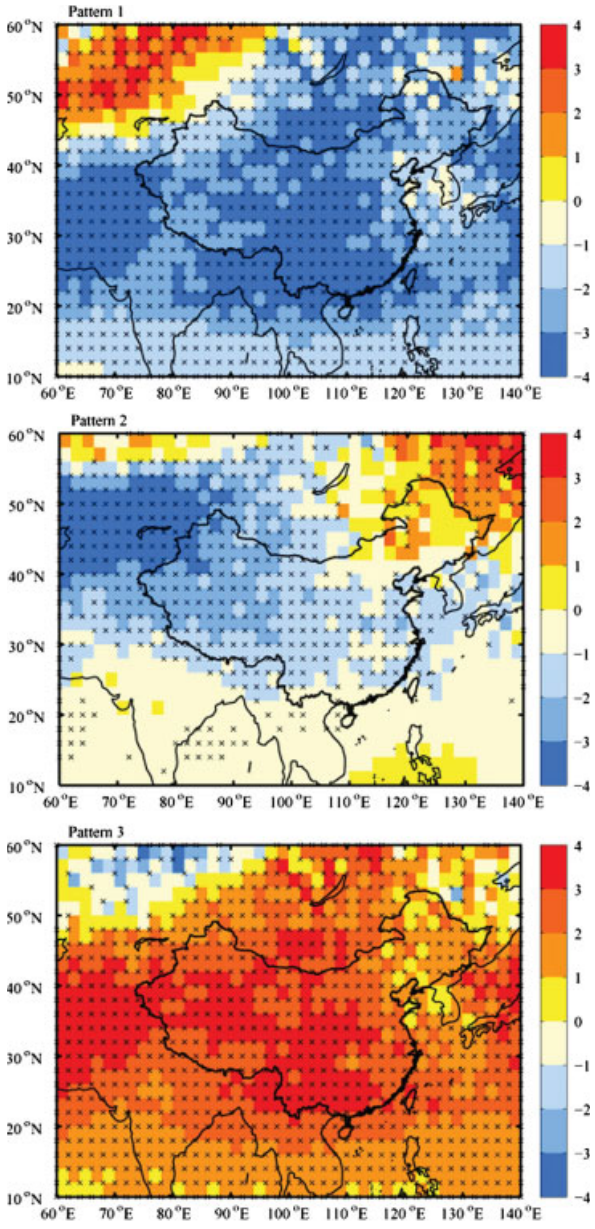

Figure 14. Atmospheric anomalous geopotential height at 500 hpa compared with the mean value (1902–2007) associated with the three patterns. 'x' indicates the geopotential height differences at the 5% significance level.

1, the negative value over China corresponds to the overall cold pattern. The geopotential height difference in the North Pacific is negative, which indicates that the Aleutian Low and East Asian trough are stronger. Furthermore, the large-scale circulation situation over Eurasia shows a high value to the west and a low value to the east. Under the control of the northwestern flow of the East Asian trough, China is obviously colder. In Pattern 2, the difference over the western part of China is negative, but it is positive over northeastern China. The west of China remains in the control of a northwesterly flow, but northeast China is under the influence of the southwesterly flow in front of the East Asian trough, causing a pattern that is cold in the west and warm in the east. In Pattern 3, the geopotential height difference is positive over the whole of China; the North Pacific region is warmer, and the East Asian Trough is weak and to the east. Zonal circulation is dominant in middle latitudes, which means that the cold airflow into China is weak and this leads to warmer temperatures.

4. Discussion

On the basis of satellite and atmospheric observations, Wielicki *et al.* (2002) and Chen *et al.* (2002) argued that the total poleward energy transport by atmosphere and ocean in the Tropics varies over decadal timescales. Marshall *et al.* (2001) argued that the net top-of-the-atmosphere radiation balance is tightly constrained, and that atmospheric and ocean energy transport should change to compensate for each other.

Figure 15 shows the Hadley circulation and vertical velocity field associated with the three patterns, which are the averages of meridional divergent flow and vertical velocity across the warm pool between 60°E and 160°W. This decadal variability in the tropical ocean shows a structure largely similar to ENSO, although this kind of structure is more prominent over the extratropical North Pacific (Zhang *et al.*, 1997). It is usually known as 'ENSO-like' mode. During the cold phase of ENSO-like mode (Pattern 1), IPWP is in warm phase (Figure 9).When IPWP is warmer, an anticyclonic anomaly circulation exists over the warm pool and the westerly/easterly in the subtropical/tropical region are greatly strengthened at 850 hPa (Zhang *et al.*, 2013). The warm water intensifies surface easterly wind anomalies in the tropics, which, in turn, strengthen the wind-driven STCs. The poleward energy transport by the ocean increases because zonal wind stresses drive poleward Ekman transport near the equator and generate subtropical cells, which carry most of the poleward ocean heat transport in the Tropics. Although the local Hadley cells in the IPWP strengthen in the cold phase of the ENSO-like mode (Figure 15(a)), the Hadley cells in the tropical Pacific weaken (Hazeleger *et al.*, 2005) and the poleward energy transport by the atmosphere decreases to compensate for the increase of the poleward energy transport by the ocean. What's more, in the cold phase of ENSO-like mode, the Aleutian Low and the East Asian Trough are strengthening, and the meridional circulation is dominated. In such circumstances, it is of benefit to cold air from the polar and high latitude move to the Southeast and makes most of China colder. The conditions in Pattern 3 are opposite to this.

For a persistent El Niño-like forcing, the poleward ocean heat transport by the meridional overturning circulation decreased, but equatorward heat transport by the gyre circulation is reduced (Hazeleger *et al.*, 2004), which will warm the warm pool, spin up the Hadley cells and the subtropical jets to shift equatorward, showing a negative

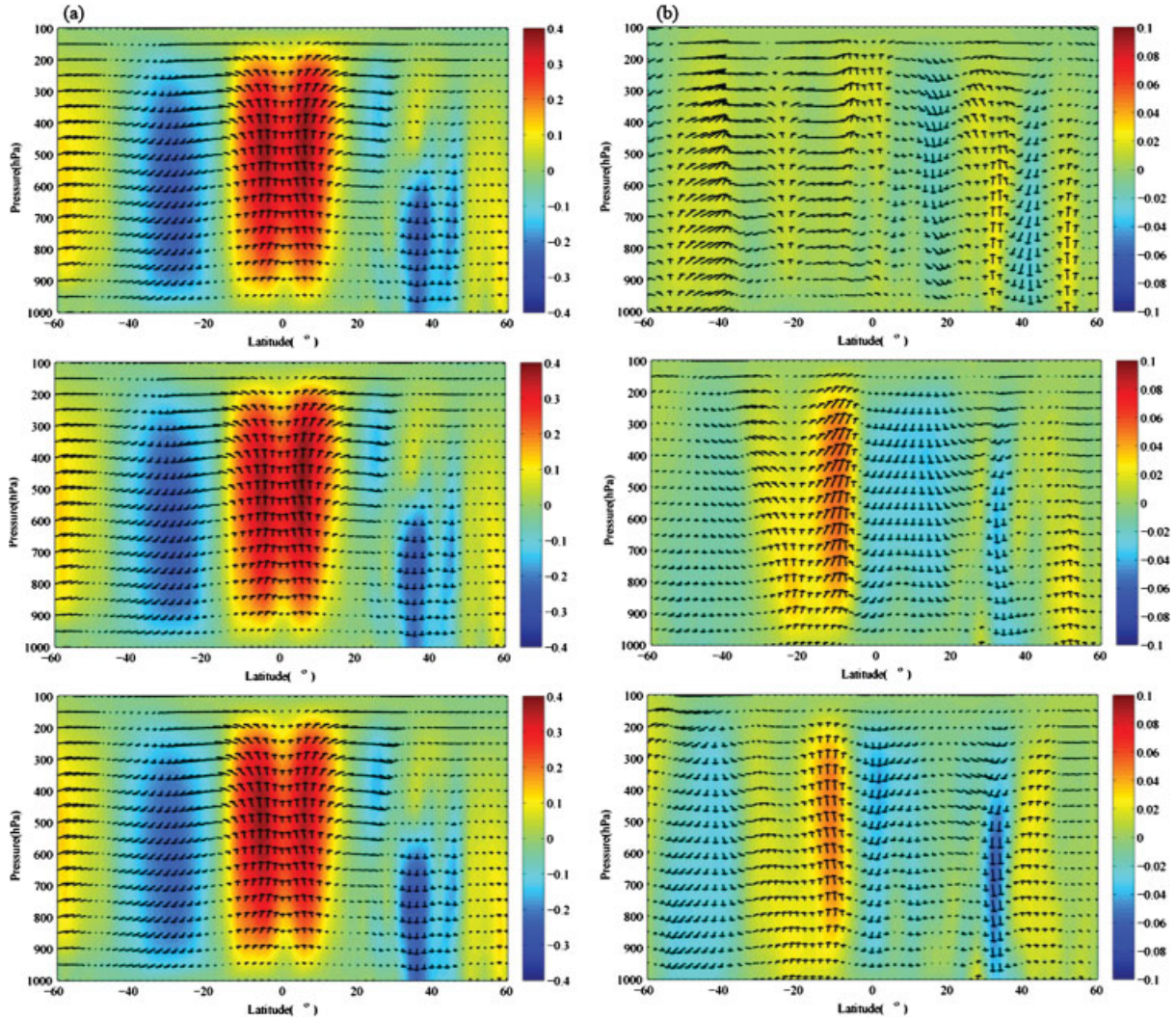

Figure 15. (a) Hadley circulation (vectors) and the negative of vertical velocity (shading) associated with the three patterns and the differences (b) relative to the mean value (1902–2007).

feedback between decadal variations in the mean meridional circulation in the atmosphere and in the Pacific Ocean (Hazeleger *et al.*, 2005; Wang and Metha, 2008).

5. Summary

First, we used the EMD–EEMD method to extract the decadal component of SAT and the four indexes of the characteristics of the IPWP. The decadal component of each SAT grid in China was then categorized into the most commonly occurring patterns of variability using the SOM clustering technique. After testing several different numbers of nodes, it was found that nine nodes provided enough patterns to cover most aspects of decadal SAT variability, while also ensuring that each node was frequent enough to provide robust statistics for comparison with the properties of the IPWP. The frequency change of each node every 10 years was also investigated and compared with the results of Wen *et al.* (2006) based on the temperature anomaly before the 1950s.

Of the nine nodes, nodes 1, 4, and 7 in Figure 2 are under a cold condition, and nodes 3, 6, and 9 are in a warm state. In nodes 2, 5, and 8 it is warm in eastern China and cold in western China. This is the same pattern obtained using the HAC clustering algorithm. To further investigate the relationship between the decadal SAT pattern in China and the IPWP, we aggregated the nine neurons into three significant types. Then, we normalized the four IPWP indexes defined in Section 2 and calculated the probability distribution when the three patterns occur. When Pattern 1 develops, the IPWP tends to have a larger volume, with its HC to the northwest and shallower. In the medium pattern (Pattern 2), the IPWP has a larger volume, and the HC is to the southeast and shallower. In the warm pattern (Pattern 3), the IPWP has a smaller volume, with its HC being located to the southeast and deeper.

The relationship between the IPWP and the decadal component of SAT in China can be summarized as follows. When IPWP is warmer (Pattern 1), surface easterly wind anomalies in the tropics are strengthened.

The IPWP shrinks westwards largely and the HC is to the west. A weaker Southern Hemisphere STC can cool and make the warm pool shallower in the Southern Hemisphere, and a stronger Northern Hemisphere STC warms and deepens the warm pool in the Northern Hemisphere, causing the HC to move to the north. The Southern Hemisphere STC is much stronger than that in the Northern Hemisphere, so the strength of the Southern Hemisphere STC can largely influence the vertical component of the HC. Therefore, the HC of the IPWP tends to be shallower. In addition, the easterly wind anomalies over the equatorial Pacific Ocean are strengthened and the poleward energy transport by the ocean increases, but the poleward energy transport by the atmosphere decreases. The Aleutian Low and the East Asian Trough are strengthened, and the meridional circulation is dominated. In such circumstances, it is of benefit to cold air from the polar and high latitude move to the Southeast and makes most of China colder. In contrast, the warm pool extends to the west during westerly wind anomalies over the equatorial Pacific Ocean (the cold phase of IPWP). This causes the trade winds to weaken and the poleward energy transport by the ocean decreases, but the poleward energy transport by the atmosphere increases. The Aleutian Low and East Asian Trough weaken, and the zonal circulation is dominant in the middle latitudes, which reduces the cold airflow into China and leads to warmer temperatures.

Acknowledgements

This work was supported by the National Basic Research Development Program of China (973 program No.2010CB950401) and the Strategic Priority Research Program of the Chinese Academy of Sciences (Grant No. XDA11010301).We would also like to thank University of East Anglia for SAT data and University of Maryland and Texas A&M University for providing the SODA data.

References

Breaker LC, Ruzmaikin A. 2011. The 154-year record of sea level at San Francisco: extracting the long-term trend, recent changes, and other tidbits. *Clim. Dyn.* **36**: 545–559, DOI: 10.1007/s00382-010-0865-4.

Cassano JJ, Uotila P, Lynch A. 2006. Changes in synoptic weather patterns in the polar regions in the twentieth and twenty-first centuries, Part 1: Arctic. *Int. J. Climatol.* **26**: 1027–1049.

Chen G, Fang LX. 2005. Improved scheme for determining the thermal centroid of the oceanic warm pool using sea surface temperature data. *J. Oceanogr.* **61**: 295–299.

Chen J, Carlson BE, Genio ADD. 2002. Evidence for strengthening of the tropical general circulation in the 1990s. *Science* **295**: 838–840.

Chen LX, Zhou X, Li W. 2004. Characteristics of the climate change and its formation mechanism in China in last 80 years. *Acta Meteorol. Sin.* **62**: 634–646 (in Chinese).

Compo GP, Whitaker JS, Sardeshmukh PD, Matsui N, Allan RJ, Yin X, Gleason BE, Vose RS, Rutledge G, Bessemoulin P, Brönnimann S, Brunet M, Crouthamel RI, Grant AN, Groisman PY, Jones PD, Kruk MC, Kruger AC, Marshall GJ, Maugeri M, Mok HY, Nordli Ø, Ross TF, Trigo RM, Wang XL, Woodruff SD, Worley SJ. 2011. The twentieth century reanalysis project. *Q. J. R. Meteorol. Soc.* **137**: 1–28, DOI: 10.1002/qj.776.

Ding YH, Dai X. 1994. Temperature variation in China during the last 100 years. *Meteorol. Mon.* **20**: 19–26 (in Chinese).

Franzke C. 2010. Long-range dependence and climate noise characteristics of Antarctic temperature data. *J. Clim.* **23**: 6074–6081.

Franzke C, Woollings T. 2011. On the persistence and predictability properties of North Atlantic climate variability. *J. Clim.* **24**: 466–472.

Gadgil S, Joseph PV, Joshi NV. 1984. Ocean-atmosphere coupling over the monsoon region. *Nature* **312**: 141–143.

Giese BS, Ray S. 2011. El Niño variability in simple ocean data assimilation (SODA), 1871–2008. *J. Geophys. Res.* **116**: C02024, DOI: 10.1029/2010JC006695.

Gong D-Y, Ho C-H. 2002a. Shift in the summer rainfall over the Yangtze River valley in the late 1970s. *Geophys. Res. Lett.* **29**(10): 781–784.

Gong DY, Ho CH. 2002b. Siberian high and climate change over middle to high latitude Asia. *Theor. Appl. Climatol.* **72**: 1–9.

Graham NE. 1994. Decadal-scale climate variability in the 1970s and 1980s: observations and model results. *Clim. Dyn.* **10**: 135–162.

Harris I, Jones PD, Osborn TJ, Lister DH. 2013. Updated high-resolution grids of monthly climatic observations-the CRU TS3.10 dataset. *Int. J. Climatol.*, DOI: 10.1002/joc.3711.

Hazeleger W, Seager R, Cane M, Naik N. 2004. How can tropical Pacific Ocean heat transport vary? *J. Phys. Oceanogr.* **34**: 320–333.

Hazeleger W, Severijns C, Seager R, Molteni F. 2005. Tropical Pacific driven decadal energy transport variability. *J. Clim.* **18**: 2037–2051.

Hu ZZ. 1997. Interdecadal variability of summer climate over East Asia and its association with 500 hPa height and global sea surface temperature. *J. Geophys. Res.* **102**: 19403–19412.

Huang NE, Wu Z. 2008. A review on Hilbert-Huang transform: method and its applications to geophysical studies. *Rev. Geophys.* **46**: RG2006, DOI: 10.1029/2007RG000228.

Huang JY, Tan BK, Suo LL, Hu YY. 2007. Monthly changes in the influence of the Arctic oscillation on surface air temperature over China. *Adv. Atmos. Sci.* **24**(5): 799–807.

Jain AK, Dubes RC. 1988. *Algorithms for Clustering Data*. Prentice Hall: Englewood Cliffs, NJ.

Jiang ZH, Tu QP, Shi N. 2001. The multi-taper spectral analysis method and its application in the global warming research. *Acta Meteorol. Sin.* **59**: 480–490 (in Chinese).

Kohonen T. 1982. Self-organized information of topologically correct features maps. *Biol. Cybern.* **43**: 59–69.

Kohonen T. 2001. *Self-Organizing Maps*. Springer: Berlin.

Liu Z. 1994. A simple model of the mass exchange between the subtropical and tropical ocean. *J. Phys. Oceanogr.* **24**: 1153–1165.

Liu Y, Weisberg RH. 2011. A review of self-organizing map applications in meteorology and oceanography. In *Self-Organizing Maps: Applications and Novel Algorithm Design*, Mwasiagi JI (ed). In Tech: Rijeka, Croatia; 253–272.

Liu Y, Weisberg RH, Moors CNK. 2006. Performance evaluation of the self-organizing map for feature extraction. *J. Geophys. Res.* **111**: C05018, DOI: 10.1029/2005JC003117.

Marshall J, Johnson H, Goodman J. 2001. A study of the interaction of the North Atlantic Oscillation with ocean circulation. *J. Clim.* **14**: 1399–1421.

McCreary J, Lu P. 1994. Interaction between the subtropical and equatorial ocean circulation: the subtropical cell. *J. Phys. Oceanogr.* **24**: 466–497.

Mitchell TD, Jones PD. 2005. An improved method of constructing a database of monthly climate observations and associated high-resolution grids. *Int. J. Climatol.* **25**: 693–712, DOI: 10.1002/joc.1181.

Neale R, Slingo J. 2003. The maritime continent and its role in the global climate: a GCM study. *J. Clim.* **16**: 834–848.

Qian C, Zhou T. 2013. Multidecadal variability of North China aridity and its relationship to PDO during 1900-2010. *J. Clim.*, DOI: 10.1175/JCLI-D-13-00235.1.

Qian C, Fu C, Wu Z, Yan Z. 2009. On the secular change of spring onset at Stockholm. *Geophys. Res. Lett.* **36**: L12706, DOI: 10.1029/2009GL038617.

Qian C, Wu Z, Fu C, Zhou T. 2010. On multi-timescale variability of temperature in China in modulated annual cycle reference frame. *Adv. Atmos. Sci.* **27**: 1169–1182, DOI: 10.1007/s00376-009-9121-4.

Qian C, Fu C, Wu Z. 2011a. Changes in the amplitude of the temperature annual cycle in China and their implication for climate change research. *J. Clim.* **24**: 5292–5302.

Qian C, Fu CB, Wu Z, Yan ZW. 2011b. The role of changes in the annual cycle in earlier onset of climatic spring in northern China. *Adv. Atmos. Sci.* **28**(2): 284–296.

Qian C, Wu Z, Fu C, Wang D. 2011c. On changing El Niño: a view from time-varying annual cycle, interannual variability and mean state. *J. Clim.* **24**(24): 6486–6500.

Reusch DB, Alley RB, Hewitson BC. 2005. Relative performance of self-organizing maps and principal component analysis in pattern extraction from synthetic climatological data. *Polar Geogr.* **29**: 188–212.

Ruzmaikin A, Feynman J. 2009. Search for climate trends in satellite data. *Adv. Adapt. Data Anal.* **1**: 667–679.

Sardeshmukh PD, Hoskins BJ. 1988. The generation of global rotational flow by steady idealized tropical divergence. *J. Atmos. Sci.* **45**: 1228–1251.

Schlesinger ME, Ramankutty N. 1994. An oscillation in the global climate system of period 65–70 years. *Nature* **367**: 723–726.

Stine AR, Huybers P, Fung IY. 2009. Changes in the phase of the annual cycle of surface temperature. *Nature* **457**: 435–440.

Sun J, Wang H, Yuan W. 2008. Decadal variations of the relationship between the summer North Atlantic Oscillation and middle East Asian air temperature. *J. Geophys. Res.* **113**: D15107, DOI: 10.1029/2007JD0096.

Tang GL, Ding YY, Wang SW, Ren GY, Liu HB, Zhang L. 2010. Comparative analysis of the time series of surface air temperature over China for the last 100 years. *Adv. Clim. Change Res.* **1**(1): 11–19.

Thomson DJ. 1995. The seasons, global temperature and precession. *Science* **268**: 59–68.

Vesanto J, Himberg J, Alhoniemi E, Parhankangas J. 2000. SOM Toolbox for Matlab 5. Report No. A57, Helsinki University of Technology. Helsinki.

Vesanto J, Himberg J, Alhoniemi E, Parhankangas J. 1999. Self organizing map. in Matlab: The SOM Toolbox. In *Proceedings of the Matlab DSP Conference*. Espoo, Finland, 34–40.

Wang S, Gong D. 2000. Enhancement of the warming trend in China. *Geophys. Res. Lett.* **27**: 2581–2584.

Wang H, Metha M. 2008. Decadal variability of the Indo-Pacific warm pool and its association with atmospheric and oceanic variability in the NCEP-NCAR and SODA reananlyses. *J. Clim*. **21**: 5545–5565, DOI: 10.1175/2008JCLI2049.1.

Wang SW, Ye JL, Gong DY, Zhu JH. 1998. Construction of mean annual temperature series for the last one hundred years in China. *Q. J. Appl. Meteorol.* **9**(4): 392–401 (in Chinese).

Wang SW, Zhu JH, Cai JN. 2004. Interdecadal variability of temperature and precipitation in China since 1880. *Adv. Atmos. Sci.* **21**(3): 307–313.

Wen XY, Wang SW, Zhu JH, Viner D. 2006. An overview of china climate change over the 20th century using UK UEA/CRU high resolution grid data. *China J. Atmos. Sci.* **30**(5): 894–903 (in Chinese).

Wielicki BA, Wong T, Allan LP, Slingo A, Kiehl JT, Soden BJ, Gordon CT, Miller AJ, Yang SK, Randall F, Susskind J, Jacobowitz H. 2002. Evidence for large decadal variability in the tropical mean radiative energy budget. *Science* **295**: 841–844.

Wood KR, Overland JE. 2010. Early 20th century Arctic warming in retrospect. *Int. J. Climatol.* **30**: 1269–1279.

Wu Z, Huang NE. 2009. Ensemble empirical mode decomposition: a noise-assisted data analysis method. *Adv. Adapt. Data Anal.* **1**: 1–41.

Wu Z, Schneider EK, Kirtman BP, Sarachik ES, Huang NE, Tucker CJ. 2008. The modulated annual cycle: an alternative reference frame for climate anomalies. *Clim. Dyn.* **31**: 823–841.

Wu R, Yang S, Liu S, Sun L, Lian Y, Gao Z. 2010. Changes in the relationship between northeast China summer temperature and ENSO. *J. Geophys. Res.* **115**: D21107, DOI: 10.1029/2010D014422.

Xie S-P, Hu K, Hafner J, Tokinaga H, Du Y, Huang G, Sampe T. 2009. Indian Ocean capacitor effect on Indo–western Pacific climate during the summer following El Niño. *J. Clim.* **22**: 730–747.

Yu R, Wang B, Zhou T. 2004. Tropospheric cooling and summer monsoon weakening trend over East Asia. *Geophys. Res. Lett* **31**: L22212, DOI: 10.1029/2004GL021270.

Zhang Y, Wallace JM, Battisti DS. 1997. ENSO-like interdecadal variability: 1900–93. *J. Clim.* **10**: 1004–1020.

Zhang ZX, Wang ZG, Li WL, Cheng G. 2013. Impacts of the SST anomalies in the Western Pacific Warm Pool on the East Asia circulation. *Meteorol. Environ. Sci.* **36**(1): 61–64 (in Chinese).

Zhu YM, Yang XQ. 2003. Relationships between Pacific Decadal Oscillation (PDO) and climate variabilities in China. *Acta Meteorol. Sin.* **61**(6): 641–654 (in Chinese).

